Applied Computing and Geosciences 27 (2025) 100263

Contents lists available at ScienceDirect

Applied Computing and Geosciences

journal homepage: www.sciencedirect.com/journal/applied-computing-and-geosciences

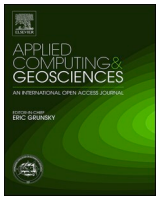

Assessing data reliability for AI-driven volcanic rock dating: A comparison of electron microprobe and laser ablation mass spectroscopy

Ali Salimian [a,*], Megan Watfa [b], Ram Grung [c], Lorna Anguilano [b]

[a] London South Bank University, UK
[b] Brunel University London, UK
[c] London Southbank University, UK

ARTICLE INFO

Keywords:
AI-Driven geochronology
Volcanic rock dating
Electron Microprobe Analysis (EPMA)
Laser Ablation Inductively Coupled Plasma Mass Spectrometry (LA-ICP-MS)
Machine learning
Trace element analysis

ABSTRACT

This study explores the integrationof artificial intelligence (AI) and modern data analytics for accurately predicting and classifying three distinct periods of volcanic activity. By leveraging previously dated volcanic samples, we assess whether existing age and geochemical data can reliably group and predict volcanic episodes. Our study focuses on the Kula Volcanic Province (Turkey). We compare the effectiveness of two analytical techniques—Electron Microprobe Analysis (EPMA) and Laser Ablation Inductively Coupled Plasma Mass Spectrometry (LA-ICP-MS)—in producing high-quality datasets for training deep learning models. While EPMA provides major and minor elemental compositions, LA-ICP-MS offers a broader range of trace elements, which may improve classification accuracy. Two experiments were conducted to evaluate the feasibility of AI-based volcanic rock age estimation. In the first experiment, an autoencoder and unsupervised clustering were applied to reduce dimensionality and group samples based on their elemental composition. The results revealed that EPMA data lacked sufficient detail to form well-defined clusters, whereas LA-ICP-MS data produced clusters that closely aligned with true age classes due to their higher sensitivity to trace elements. In the second experiment, a deep neural network (DNN) was trained to classify rock ages. The LA-ICP-MS-based model achieved a classification accuracy of 95 %, significantly outperforming the EPMA-based model (72 %). These findings underscore the importance of data quality and analytical technique selection in AI-powered geochronology, demonstrating that high-quality trace element data enhances AI model performance for volcanic rock age estimation.

1. Introduction

Volcanic rocks, a type of igneous rock, form from the cooling and solidification of magma or lava at or near Earth's surface. These rocks are intrinsically linked to volcanic activity and manifest in various forms, including lava flows, volcanic cones, and ash deposits. Their study is pivotal for unravelling Earth's geological history, as they provide critical evidence for understanding volcanic and tectonic processes.

Serving as a direct link to Earth's interior, volcanic rocks offer a unique window into the mechanisms of magma generation, differentiation, and eruption. They are fundamental to decoding Earth's dynamic geological processes, revealing key insights into volcanic activity, tectonic movements, and the evolutionary history of the planet. The diverse composition of volcanic rocks, ranging from basaltic to rhyolitic, reflects variations in source material, chemical composition, and tectonic settings (Irvine and Baragar, 1971; Le Bas et al., 1986).

Radiometric age dating is a cornerstone technique in Earth sciences, enabling determination of the absolute ages of rocks and geological events through the measurement of isotopic decay. Geochronology, the scientific discipline dedicated to determining the age of rocks, minerals, and geological events, provides both absolute and relative temporal frameworks essential for reconstructing Earth's history, particularly critical in the study of volcanic systems for several reasons:

- To determine the timing of eruptions
- Constrain the recurrence interval of eruptions for hazard assessment
- Understanding magmatic history
- Reconstructing past climates

Traditionally, radiometric dating has been regarded as the benchmark technique for age determination due to its unparalleled reliability and precision in providing absolute age measurements. Methods such as

* Corresponding author.
E-mail address: salimiaa@lsbu.ac.uk (A. Salimian).

https://doi.org/10.1016/j.acags.2025.100263
Received 20 March 2025; Received in revised form 6 June 2025; Accepted 30 June 2025
Available online 5 July 2025

uranium-lead (U-Pb) and rubidium-strontium (Rb-Sr) isotopic dating have long been the gold standard in geochronology, offering highly accurate insights into the geological history of rocks. However, these techniques are inherently resource-intensive, necessitating significant sample preparation, specialized laboratory facilities, and sophisticated instrumentation. The complexity of these methods not only drives up costs but also limits their accessibility, particularly for smaller or underfunded research institutions. As a result, researchers often seek alternative approaches, such as utilizing geochemical proxies in conjunction with machine learning models, to infer rock ages (Petrelli et al., 2017). These methods, while not replacing radiometric dating, can provide efficient and cost-effective solutions for exploratory studies and complement traditional geochronological techniques. The implementation of artificial intelligence (AI) represents a significant step toward optimizing the use of modern characterisation techniques in the study of volcanic materials. For example, recent studies have explored advanced computer vision models for rock analysis and classification (Sim et al., 2022), while others have combined approaches such as rough set mathematical theory with machine learning (ML) models for classification (Shaaban and Tawfik, 2020). One of the primary advantages of ML in geochronology is its ability to quickly and accurately process large datasets. While traditional radiometric methods can take weeks to months to yield results, ML models, once trained, can provide near-instantaneous age predictions for volcanic rocks, significantly accelerating research timelines (Pignatelli and Piochi, 2021). This rapid prediction capability is especially valuable in areas with active volcanic activity, where it can support faster decision-making for hazard mitigation and emergency response (Ouzounis and Papakostas, 2021). Recent studies have increasingly applied AL and ML in Earth science to enhance the accuracy of geochronological analysis, for example Petrelli et al. (2017) combined ML algorithms with microanalysis data and large geochemical datasets to constrain Pleistocene magmatism. Similarly, Uslular et al. (2022) applied ML models to classify and correlate tephra from Plio-Quaternary volcanic fields, showcasing the potential for data-driven approaches.

ML refers to a system's ability to predict a pattern in data and make assumptions without explicit programming (Das et al., 2020). ML relies on identifying common characteristics within a dataset to classify or predict outcomes. Proper feature selection is critical, as failure to select relevant features can lead to errors and reduce learning effectively. ML is revolutionising access to advanced geochemical techniques by minimizing the reliance on expensive radiometric equipment. This democratization of technology allows smaller research institutions to engage in cutting-edge geochronology using ML models on relatively simple computing systems, providing sufficient training data is available. Such increased accessibility promotes broader collaboration across institutions and regions, enhancing the scope and depth of geological studies. In addition to improving efficiency, ML excels in identifying patterns and trends in volcanic data that traditional methods may overlook. Through advanced algorithms, subtle relationships between elemental compositions and rock ages can be revealed, offering new insights into volcanic processes. ML has also enhanced the accuracy of mineral provenance and deposit classification, with techniques such as random forests and neural networks refining exploration efforts in complex geological contexts (Zhang et al., 2023).

Electron Microprobe Analysis (EPMA) and Laser Ablation Inductively Coupled Plasma Mass Spectrometry (LA-ICP-MS) are advanced compositional data acquisition techniques that yield detailed datasets on the elemental and isotopic compositions of volcanic rocks (Jenner and O'Neill, 2012; Gennaro et al., 2023). EPMA uses a focused electron beam to analyse a sample's chemical composition best for major and minor elements (>0.1 wt percent (wt%)), while LA-ICP-MS employs lasers to ablate material, measuring trace elements (<100 parts per million (ppm)) as well as isotopic compositions, although the focus on this study is on trace elements only. These techniques generate high-resolution geochemical data, essential for age inference. However, the manual interpretation of such large and complex datasets is labour-intensive and susceptible to error, which makes ML an ideal tool for automating this process by identifying patterns in high-dimensional data. By training ML models on compositional data derived from EPMA and LA-ICP-MS analysis of samples with known ages, it becomes feasible to predict the ages of new volcanic rock samples more efficiently once their compositions are measured. These models are particularly suited for age classification due to their robustness in handling complex, non-linear relationships (Ouzounis and Papakostas, 2021; Pignatelli and Piochi, 2021).

Geochronology encompasses a sub-discipline called petrochronology, which is rapidly gaining prominence in Earth sciences. This field focuses on linking time with specific rock-forming processes and their associated physical conditions (Engi et al., 2017). Petrochronology investigates the temporal evolution of rocks by analysing mineralogical and chemical signatures, integrating petrographic, geochemical, and geochronological methods to understand the timing and processes involved in the formation and alteration of volcanic rocks.

As petrochronology generates a vast amount of geochemical data, is it natural to leverage the advancements in AI to extract deeper insights from this geological data (Schmidhuber, 2022). AI is increasingly applied in mineral exploration, using techniques such as computer vision, remote sensing, and geochemical analysis to enhance data interpretation and decision-making (Yang et al., 2024). The fusion of AI with petrochronology holds immense potential for advancing our understanding of Earth's geological processes (Kohn and Penniston-Dorland, 2017; Walters et al., 2022).

While ML has transformative potential in geoscience, several critical research gaps hinder its broader implementation. A key challenge is the limited diversity and global representativeness of existing datasets, reducing ML model robustness and applicability across a range of geological settings. Reliance on existing data introduces regional biases, missing values, and inconsistencies that can skew results. Addressing these issues requires the development of standardised, high-quality, globally representative geochemical databases to ensure consistency and reliability. Another limitation is the lack of integration across multidisciplinary data, such as geochemical, isotopic, petrographic, and geochemical variables. Current models fail to fully capture the complexity of geological processes. For example, understanding magmatic and mineralogical systems demands multi-phase, multi-proxy datasets for holistic modelling. But does combining diverse data sources enhance the accuracy and interpretability of ML-based predictions?

Methodological challenges further impede progress. These include handling imbalanced datasets, improving algorithm transparency, and expanding model applicability to diverse geological contexts. Future research should explore advanced ML techniques, such as neural networks, to enhance the reliability and resilience of predictive models.

This study aims to investigate whether it would be suitable to use data generated from various laboratories, each employing different brands of equipment and calibration policies, for training AI models, assuming a universal bank is to be created. Ultimately, an AI model's performance is as good as the quality of the data it is trained with.

1.1. AI context and relevance of selected algorithms

Artificial Intelligence (AI) is a multidisciplinary domain aimed at building systems capable of performing tasks that would typically require human intelligence, such as learning, reasoning, pattern recognition, and decision-making. Within AI, machine learning (ML) has become a dominant approach, enabling computers to identify patterns in data and improve performance over time without being explicitly programmed. A powerful subfield of ML is deep learning, which uses layered neural network architectures to model highly complex, nonlinear relationships. These methods have revolutionised fields such as medical imaging, natural language processing, and remote sensing, and are increasingly being adopted in geosciences for analysing high-

dimensional datasets and supporting decision-making.

The algorithms used in this study — including autoencoders, clustering models, and supervised deep neural networks (DNNs) — are core components of the modern AI landscape. Autoencoders, as part of deep learning, are ideal for unsupervised representation learning and dimensionality reduction, enabling the extraction of latent features from complex geochemical datasets. Clustering algorithms were applied to this latent space to explore unsupervised groupings of rock samples. DNNs, on the other hand, exemplify how AI models can learn predictive relationships from labelled data — in this case, predicting rock age categories from geochemical signatures. These techniques demonstrate how the principles of AI can be applied to geological and petrochronological challenges, offering novel and scalable alternatives to traditional analytic workflows.

2. Methodology

In this study, we obtained volcanic rock samples from different localities across a volcanic site in Turkey. We analysed the age of the rocks and then carried out a quantitative analysis of the elemental compositions of the rocks using two separate characterisation techniques.

2.1. Introduction to study site

Turkey is a tectonically and volcanically active region situated on the boundary between the Eurasian Plate, the African Plate, and the Arabian Plate (Tokçaer et al., 2005) (Fig. 1). The positioning of this makes the area vulnerable to intense seismic and volcanic activity, which has shaped its diverse geomorphological landscape with many processes occurring such as subduction, collision, and strike-slip faulting as a result of the interactions between these tectonic plates over tens of millions of years. Anatolia, also known as Asia Minor, is a large peninsula in Western Asia comprising most of modern-day Turkey. This area is in the collision zone between the African, Arabian, and Eurasian plates, and is bounded by the Mediterranean Sea to the south, the Aegean Sea to the west, the Turkish Straits to the northwest, and the Black Sea to the north.

In Western Anatolia, the Kula Volcanic Province (KVP) is a prominent volcanic terrane and represents the westernmost and youngest volcanism in Turkey. This area is a 15 km north-south, and 40 km east-west monogenetic volcanic field (MVF), hosting a range of diverse geomorphological features and landforms including lava flows, cinder cones, lava caves, maars, and columnar basalts. The volcanic rocks of this area have been divided into 3 groups based on their petrological, geochemical, and geochronological characteristics, referred to as first stage, second stage, and third stage in decreasing ages, and represent three different active volcanic phases in the Quaternary Period.

2.2. Importance of Monogenetic Volcanic Fields (MVFs)

Monogenetic Volcanic Fields (MVFs) are found in diverse tectonic settings worldwide, where small batches of magma can erupt effusively and/or explosively for weeks to decades, with monogenetic volcanism producing small-volume volcanoes, typically <1km3. Volcanic vents represent the pathway for magma to the upper mantle, with an eruption forming a vent in an unknown location. This type of volcanism usually consists of clusters of volcanoes dispersed over a large area. As the term suggests, monogenetic volcanoes consist of singular eruptions, which

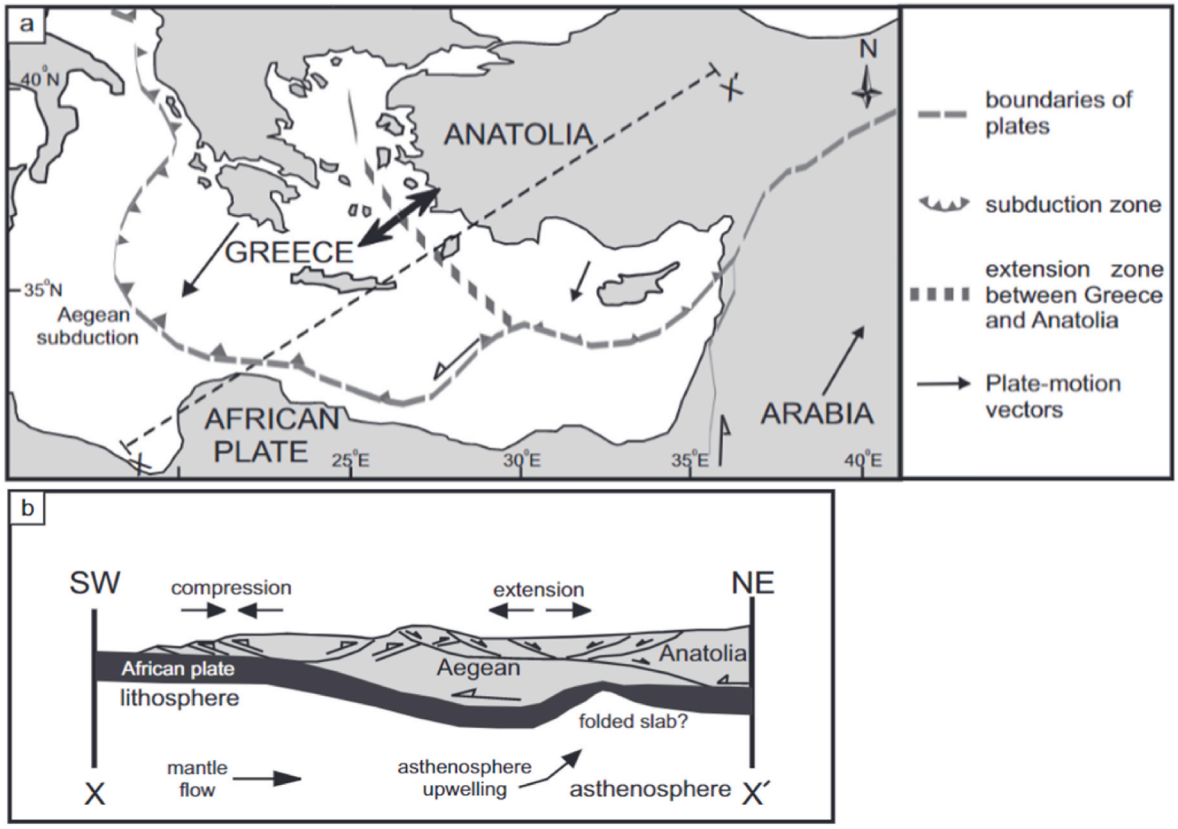

Fig. 1. (a) Tectonic model showing plate tectonics and direction of movement. This movement is the driving force behind the geodynamic factors shaping western Anatolia. The figure shows the African plate (Cyprus-Aegean subduction zone) subducting beneath the Greek and Anatolian microplates, resulting in an extensional margin between the Aegean Sea and western Anatolia (thick double arrow). Thin arrows represent the plate motion at present; (b) cross-section of the tectonic model shown in a, representing the split of the Greek and Anatolian plates and the window into the underlying stretched slab that would allow melting and ascent of volcanic material (Doglioni et al., 2002; Tokçaer et al., 2005).

means if an eruption stops, volcanism will not occur at the same eruptive centre again. Volcanism in the area may still be active however and may occur as newly developed eruptive centres within its monogenetic field. Due to their unpredictable eruptive nature, the origin, longevity, and temporal-spatial distribution of eruptive centres are poorly understood (Jaimes-Viera et al., 2018). Due to the abundance of MVFs in every tectonic environment, this form of volcanism represents a localised and unpredictable hazard in heavily populated areas within proximity. There is a lack of understanding of MVFs particularly linked to the duration between eruptions which often results in the lack of detailed geochronologies making the evolution of these features often difficult to study. Understanding how and when such volcanism occurs, as well as insights into the physical-chemical parameters of magma is essential to understand these events.

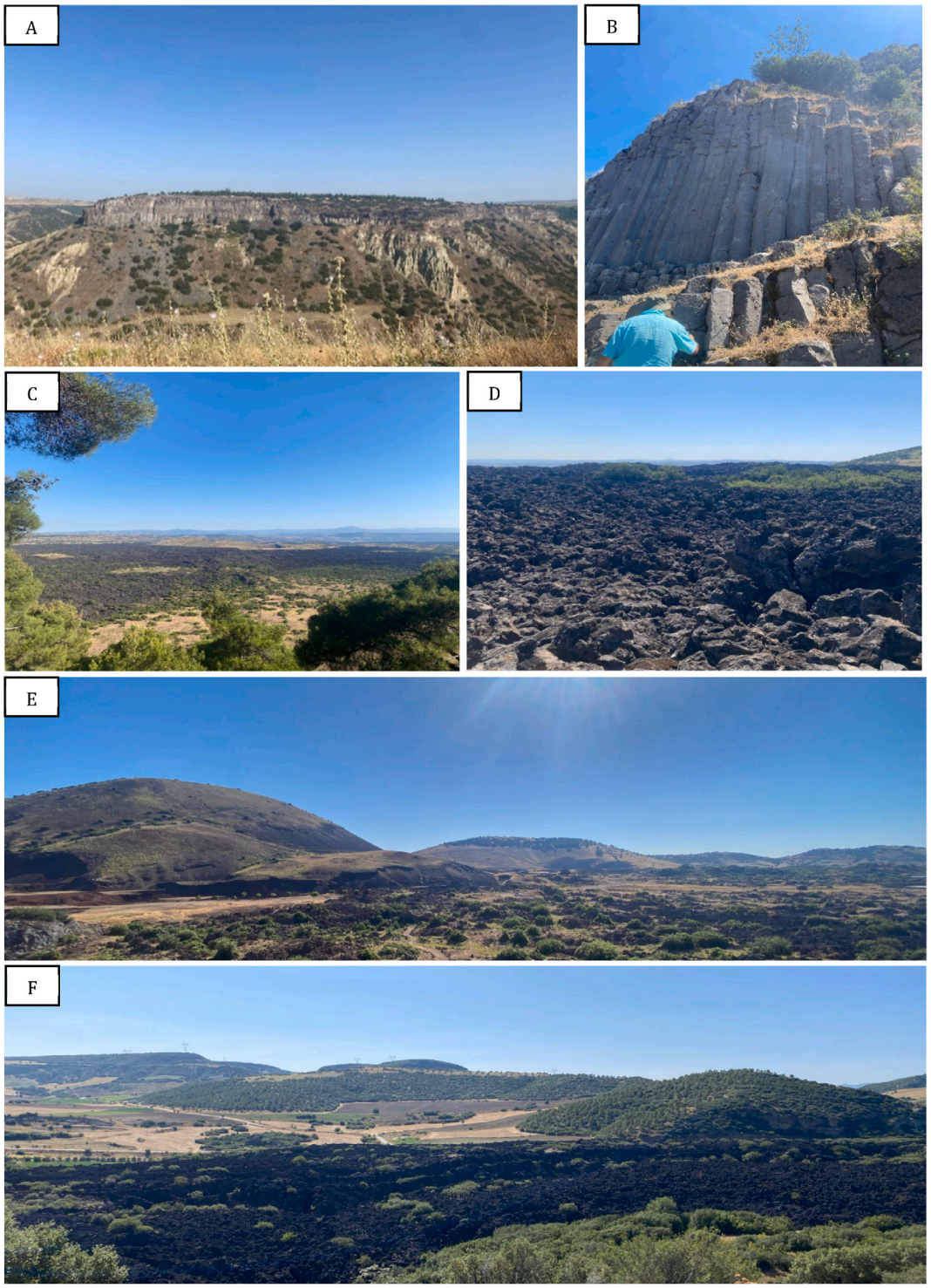

Fig. 2. Field photographs of the KVP. a) Looking west toward the first stage plateau with lava flow forming erosion-resistant caps; b) first stage columnar basalts formed as a result of rapid lava cooling, demonstrating well-defined vertical jointing; cd) extensive lava flows of the third stage; e) view northeast displaying numerous volcanic cones from the second and third stage; f) view east showing third stage lava in the foreground, with volcanic cones from the second stage in the background.

2.3. Sampling

The data utilised in this study constitutes a subset of a broader PhD research project. Sampling was carried out during a field visit in 2023, during which 39 samples were systematically collected from varying volcanic material, including cinder cones, lava flows, and other pyroclastic material such as ash deposits (Fig. 2). Sampling locations (Fig. 3) were strategically selected based on criteria including accessibility, visible stratigraphy, and spatial distribution of lava flows and volcanic deposits, as identified through remote sensing data, and previous geological maps.

2.4. Characterization techniques

Once samples were collected, data was gathered via EPMA and LA-ICP-MS techniques, followed by evaluating the age of the samples using Ar/Ar dating.

EPMA and LA-ICP-MS are powerful tools for investigating and understanding the composition of rocks found in volcanic complexes. These techniques enable detailed geochemical analyses of volcanic materials, uncovering critical information about subsurface processes that may not be apparent from surface observations. This is particularly significant for MVFs, where surface variability often reflects complex and diverse underlying processes. Volcanic deposits serve as natural records of magmatic processes, reflecting both physical and chemical changes that occur throughout the magma's journey-from its residence in the crustal plumbing system to its final cooling at the Earth's surface (Oggier et al., 2023). Magma composition plays a crucial role in determining physical properties such as viscosity, density, and eruption style, which can later be used for long-term evaluations of hazard and risk.

Major elements are those that define a rock's mineralogical makeup, for example, Si, Al, Ca, Mg, Na, K, Ti, Fe, Cr, Mn, and P (Refer to Supplementary Data). These elements, together with O compose approximately 95 % of the earth's crust and are crucial for rock classification. Trace elements, in contrast, are those present in much smaller concentrations, usually less than 0.1 %. Examples include Ni, Cu, Y, Co, Sr, Cr, Rb, Zr, Zn, Nb, Sc, Ga, Th, Ba, Li, Ce, V, Nd, Pb, Pr, La, U, Eu, Er, Ho, Yb, Gd, Hf, Dy, Lu, Tm, and Tb (Refer to Supplementary Data Table 2).

Trace element data provides important clues regarding volcanic origin and evolution. While all elements provide valuable information, trace elements exhibit a wider range of chemical behaviours due to their diverse positions in the periodic table, compared to the relatively constrained variability of major elements (Doglioni et al., 2002). These elements are highly sensitive to changes in temperature (T), pressure (P) and the chemical environment during magma formation and ascent, making them powerful indicators of magmatic processes and their underlying dynamics.

In EPMA analysis, various approaches can be employed including spot analysis at specific points within a mineral grain (eg; core, intermediate, rim), core-to-rim profiles, and elemental mapping. Each method offers valuable insight into mineral chemistry. This study focuses on spot analysis, providing high-precision elemental concentrations at different locations within a crystal. This approach is particularly effective for examining mineral zoning and understanding the chemical evolution of mineral grains. The core, being the earliest part of the mineral to crystallise, reflects the initial conditions of the melt during the early stages of formation. The intermediate zone represents the transition between the core and the rim and often shows gradual and/or abrupt changes in composition due to changes in magma composition, T, or P, reflecting processes such as magma mixing, or the introduction of new material. The rim, as the last to crystalise, captures the final stages of mineral growth, often revealing information on later alteration occurrences. This can provide information about cooling and magma solidification.

After EPMA was used to determine the major and minor element compositions of a sample, LA-ICP-MS was performed to analyse trace elements with high precision and sensitivity using precise spot analysis. As with EPMA, multiple spots, in this case, the core, intermediate, and rim were followed to match those carried out by EPMA. This sequential approach ensures a thorough geochemical analysis, combining the major and minor elements using EPMA, with the trace elements using LA-ICP-MS.

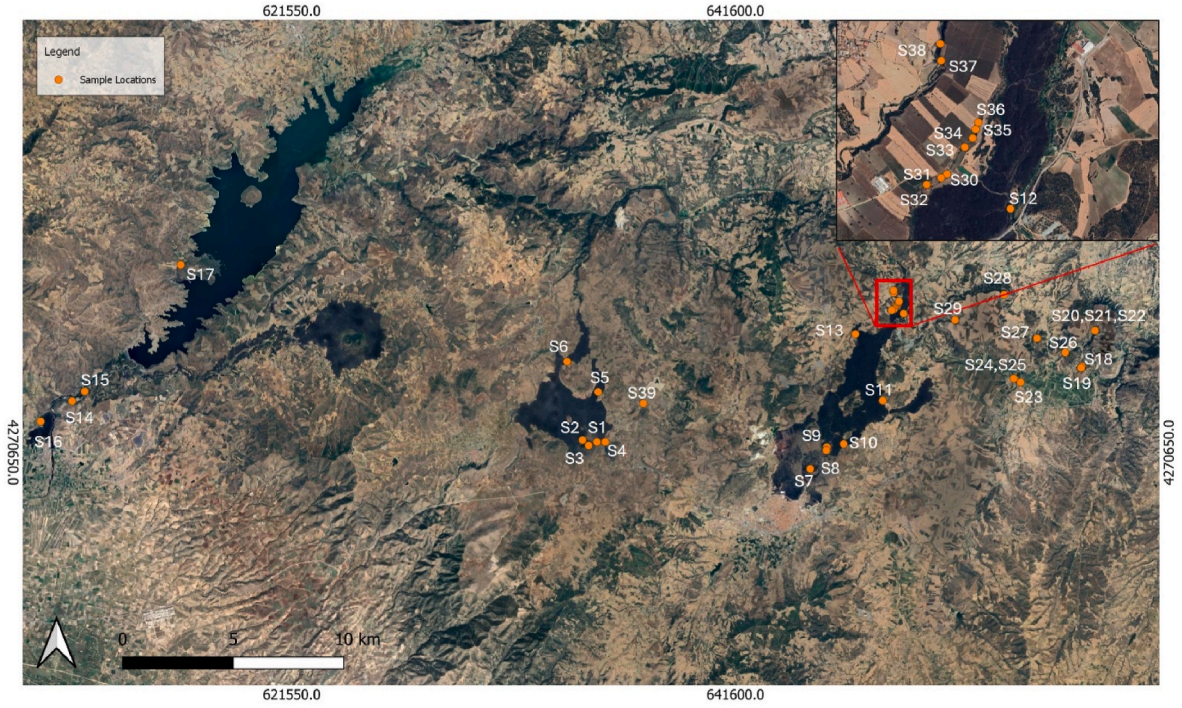

Fig. 3. Location map of the study area showing the distribution of samples collected with sample names. For this study, the geochemical data was used from 12 samples (S4, S6, S7, S16, S20, S21, S24, S25, S30, S32, S36, S37) (Refer to Supplementary Data Table 1).

2.5. Age prediction

Dating methods can be specifically tailored to suit different rock types, geological conditions, and timescales, ensuring accurate dating across a wide range of materials. The selection of the appropriate method depends on factors such as the half-life of the radioactive isotopes and the minerals present in the rocks. Common examples of radiogenic dating techniques include uranium-lead (U-Pb), rhubidium-strontium (Rb-Sr), radiocarbon dating (Carbon-14), fission track dating, rhenium-osmium (Re-Os), potassium-argon (K-Ar), and argon-argon ($^{39}Ar/^{40}Ar$). For a more comprehensive discussion, readers are directed to the literature (Condomines et al., 2003; Reiners et al., 2005; Coble et al., 2017; Danišík et al., 2017; Reyes-Guzmán et al., 2018; Zawacki et al., 2022; Lee et al., 2024). In the context of volcanology, the most suitable methods are K-Ar or $^{39}Ar/^{40}Ar$, which are particularly effective for three key reasons:

1) they target specific minerals common in igneous rocks, such as feldspar, mica, and amphibole,
2) ^{40}K has a decay half-life of 1.25 billion years (Di Vincenzo, 2022), meaning that the measured 40Ar can measure a wide range of timescales, and
3) they are capable of accurately dating material as young as the Late Holocene (Schmitt et al., 2013).

Ar-Ar offers higher precision by irradiating samples to convert ^{39}K to ^{39}Ar and measuring the ratio of ^{40}Ar to ^{39}Ar (Merrihue and Turner, 1966; McDougall and Harrison, 1999). The sample is irradiated in a nuclear reactor to convert a portion of the stable isotope ^{39}K to ^{39}Ar, allowing the $^{39}Ar/^{40}Ar$ ratio to be measured directly. This method involved step-heating, allowing for the release of argon in increments (Di Vincenzo, 2007). This method uses the step-heating approach and can identify argon loss, excess argon, or trapped argon from a previous event resulting in reliable age determinations (Renne et al., 1998). The step-heating can detect multiple argon release patterns, revealing if separate parts of the sample crystallised differently. While Ar-Ar dating is a robust method, sample preparation is very important, with samples needing to be fresh, with little/no alteration otherwise this can complicate the age interpretation. This method requires more specialized equipment, including nuclear reactors and mass spectrometers, and can therefore be less accessible to some facilities.

2.6. Clinopyroxene and mineral characteristics

In volcanic rocks, the term ‘zoning’ refers to the spatial variation in the composition of a single mineral grain (Ginibre et al., 2007). These variations typically appear as distinct layers or regions within the crystal and record the physical and chemical changes of the liquid phase during crystal growth (see section 2.4). Mineral zoning is observable through optical microscopy (Fig. 4) and in back-scattered electron (BSE) images via EPMA (Fig. 5).

Different types of mineral zoning, such as concentric, hourglass, and oscillatory, reflect the various growth conditions. Readers are directed to the literature for a detailed explanation of the different mineral zoning patterns (36). Textural and compositional variations associated with mineral zoning can provide critical insights into magmatic histories and can be used to decipher magmatic processes leading to an eruption (MacDonald et al., 2024). In geochemical analysis, mineral zoning is valuable for understanding the timing and nature of processes such as magma mixing, cooling, and fractional crystallisation.

EPMA and LA-ICP-MS employed on the mineral phase clinopyroxene (cpx), which is an important silicate mineral found in a wide range of igneous and metamorphic rocks. Its composition and structure make it a highly informative mineral to study as it can accommodate a variety of

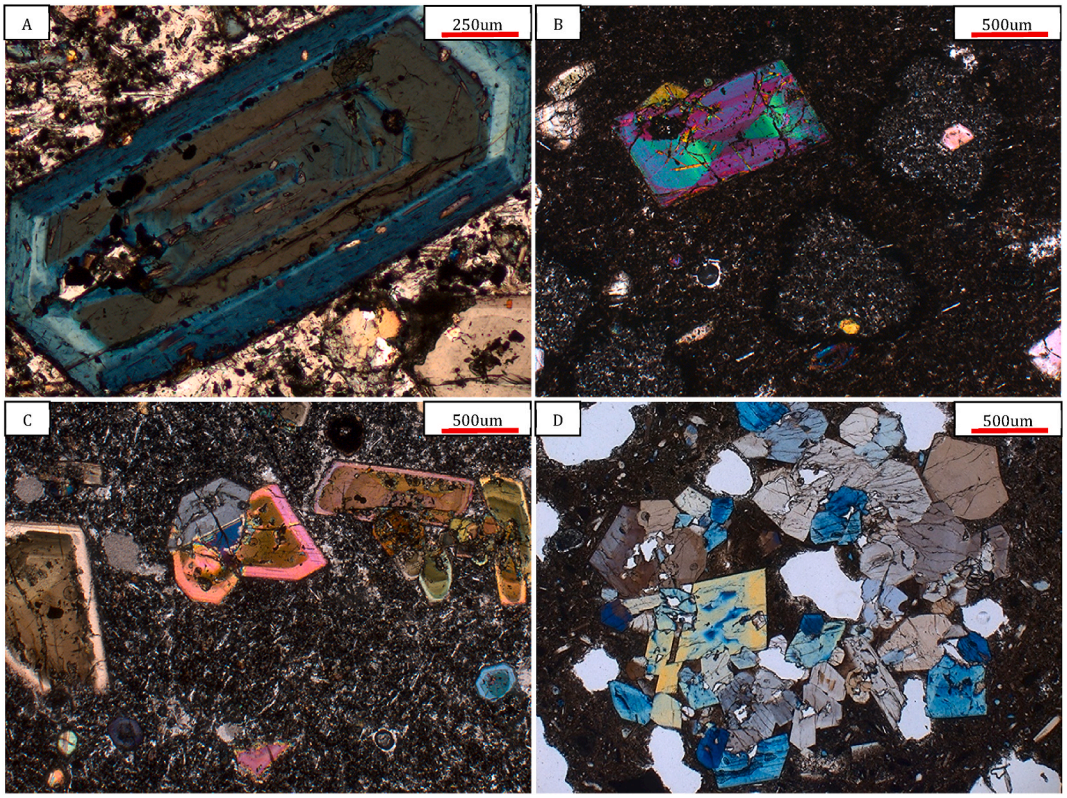

Fig. 4. Photomicrographs in cross-polarised light (XPL) showing different mineralogical and textural features. a) First stage euhedral cpx crystal showing concentric zoning with distinct rings of varying composition; b) second stage euhedral cpx crystal showing hourglass zoning; c) several second stage euhedral cpx crystals showing concentric zoning; d) third stage euhedral and subhedral cpx and ol crystals showing a glomeroporphyritic texture.

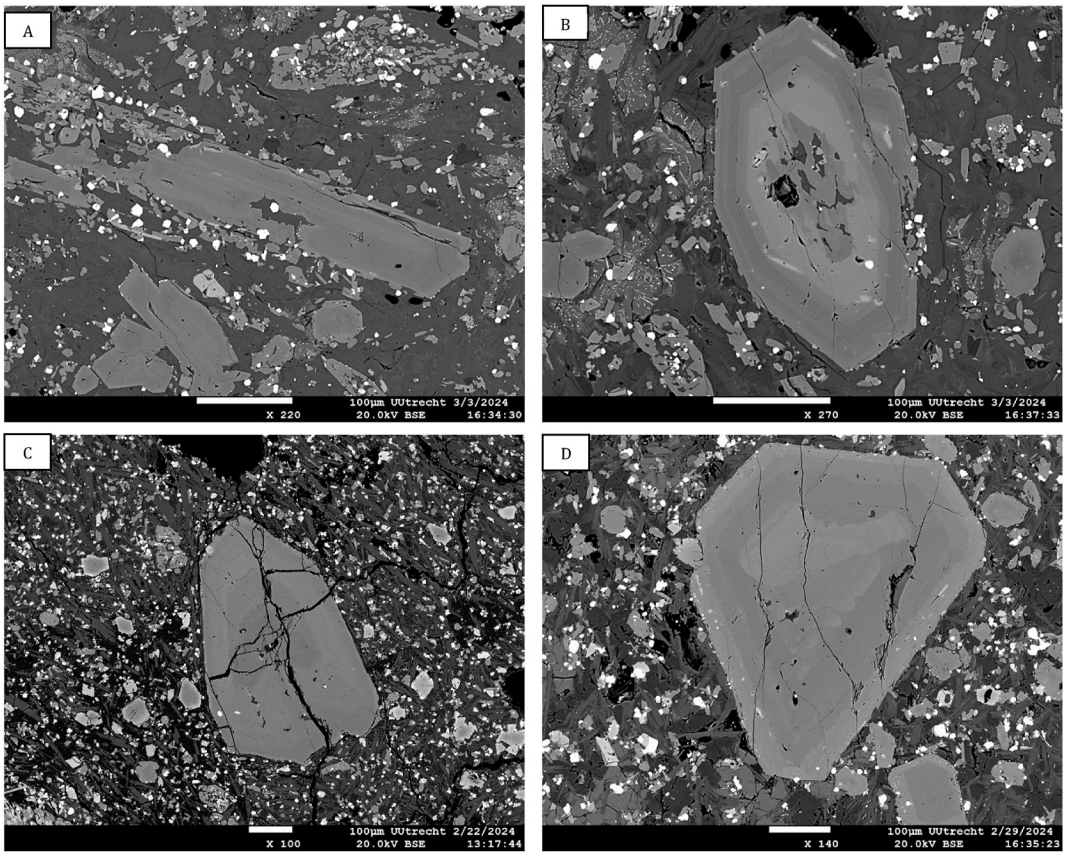

Fig. 5. EPMA backscattered electron (BSE) images of cpx crystals displaying mineral zoning. Distinctive compositional zones can be seen which highlights the various chemical variations. ab) Third stage samples; cd) First stage samples.

major and trace elements which reflect T, P, and magma compositional variations. Cpx is a calcium-magnesium-iron silicate which consists of chain silicates with the general formula Ca (Mg, Fe) Si2O6. They can vary in composition depending on the relative proportions of Ca, Mg, and Fe, resulting in common mineral types of diopside CaMgSi2O6 and augite (Ca, Na) (Mg, Fe, Al, Ti) (Si, Al)2O6).

An important indicator of magma evolution can be calculated from the data derived from EPMA analysis of cpx minerals, known as the magnesium number, or Mg#. The Mg# is the ratio of Mg to the total Fe and can be calculated with the following equation:

$$Mg\# = 100 \text{ x } Mg / Mg + Fe2+$$

Higher Mg# values reflect more primitive, mantle-derived magmas with higher Mg content, while lower Mg# values suggest more evolved magmas enriched in Fe due to fractional crystallisation. During this process, early formed Mg-rich minerals such as olivine (ol) crystallise out, leaving the remaining melt Fe-enriched. Mg# is valuable for comparing samples, modelling fractional crystallisation processes, and performing thermobarometry calculations to estimate T and P of cpx crystallisation. Although this study does not delve deeply into the Mg#, it is important to understand the significance of this geological parameter, and how it can be determined through EPMA analysis.

2.7. Laboratory

Geochemical analysis requires high-quality, polished thin sections prepared to a thickness of 30 µm and further polished using 0.25 µm diamond suspension to achieve a smooth sample surface free from scratches or imperfections. This ensured minimal interference during electron beam-based analysis. For EPMA, samples must be carbon coated with a 20–30 µm layer to enable high-resolution imaging and qualitative analysis by establishing conductivity between the electron beam and the sample surface. Without this, non-conductive samples may accumulate electrical charge, leading to distorted signals and poor image quality. For LA-ICP-MS carbon coating is not necessary as it relies on a laser rather than electron conductivity, eliminating the risk of charging. Samples under the laser beam are required to be free from contamination.

Major element compositions were acquired using EPMA from four different laboratories:

- The GeoLab at the Faculty of Geoscience, Utrecht University
- The Faculty of Sciences of the University of Lisbon
- The Department of Earth Sciences, University of Cambridge
- The Sorby Centre for Electron Microscopy, University of Sheffield.

While each laboratory followed the same methodology, slight variations in operating conditions, standards, and operating crystals were chosen (Refer to Supplementary Data Tables 3–7). Calibrations were performed using a range of well-characterised mineral standards corresponding to the elements of interest (Refer to Supplementary Data Tables 3–7). To ensure the accuracy and precision of the measurements, the instrument was calibrated at the beginning and end of each session daily, and standard materials were periodically reanalysed to monitor potential instrumental drift. Matrix effects were corrected using the ZAF method (accounting for atomic number (Z), absorption (A), and fluorescence (F)) at the Utrecht, Cambridge, and Lisbon laboratories, while the PRF correction method (incorporating primary (P), rear (R), and focusing (F)) was applied at the Sheffield laboratory.

Trace element analyses were performed at the Department of Earth Sciences “A. Desio” of the University of Milan using an Analyte excite 193 nm ArF excimer laser coupled with a Thermo Fisher Scientific iCAP-

RQ mass spectrometer. Unlike the EPMA analysis, the data for trace element analysis was acquired from a single laboratory. The operating conditions were the following for cpx: 6 J/cm2 fluence, 40 μm and 10 Hz repetition rate. The acquisition time was 60 s on the sample and 40 s on the background. Data reduction was carried out with the software package GLITTER (Griffin, 2008) using CaO wt% concentrations from microprobe analyses as an internal standard. The international reference material BCR-2G (Jochum et al., 2005) was used as a calibration standard and reference glasses (NIST612 (Pearce et al., 1997); ARM-3 (Wu et al., 2019); GSD-2G and ATHO-G (Jochum et al., 2005), were used to monitor accuracy. The reproducibility is less than 20 % for most elements.

Four samples, S6, S11, S27, and S36 (Fig. 6 and Supplementary Data Table 1) were subject to Ar-Ar dating carried out at the Ar-Ar Geochronology Laboratory, CNR, Pisa, Italy. The samples were crushed and sieved by hand using a pestle and mortar, and fragments between 0.25 and 0.5 μm were observed under the microscope to remove the grains for analysis, by handpicking fresh, unaltered groundmass. During the sample preparation, samples were worked mechanically by hand to avoid contamination, and no solvents or substances were used during the preparation of the material. For the Ar-Ar method, readers are referred to (Smellie et al., 2022) for a detailed methodology of the technique.

A limited mini data bank was created based on the activities discussed. These data ultimately reflect the elemental analysis of our samples associated with their measured age.

2.8. Data obtained via the Ar/Ar analysis

The results show the first stage sample is 1264.5 +- 9.2 Ka, the second stage sample is 179 +- 8.7 Ka, and the third stage samples are 4.3 +- 6.1 Ka and 3.5+- 7.6 Ka (Fig. 6). The results show three distinct phases of activity all within the Quaternary Period and date as the Early Pleistocene (first stage), the Middle Pleistocene (second stage), and the Holocene (third stage).

The values from dating represent the time that has passed since the rock last cooled and solidified, effectively corresponding to the time of the volcanic eruption. The value following the +- symbol represents the analytical uncertainty, or error, for each date. Larger errors suggest that samples may have encountered complexities such as alteration, argon loss, or contamination which give a broader timeframe and less precise age determinations. Smaller errors may result from a more stable argon retention, possibly as these samples have not experienced argon loss over time and therefore provide more exact timing. For the third stage,

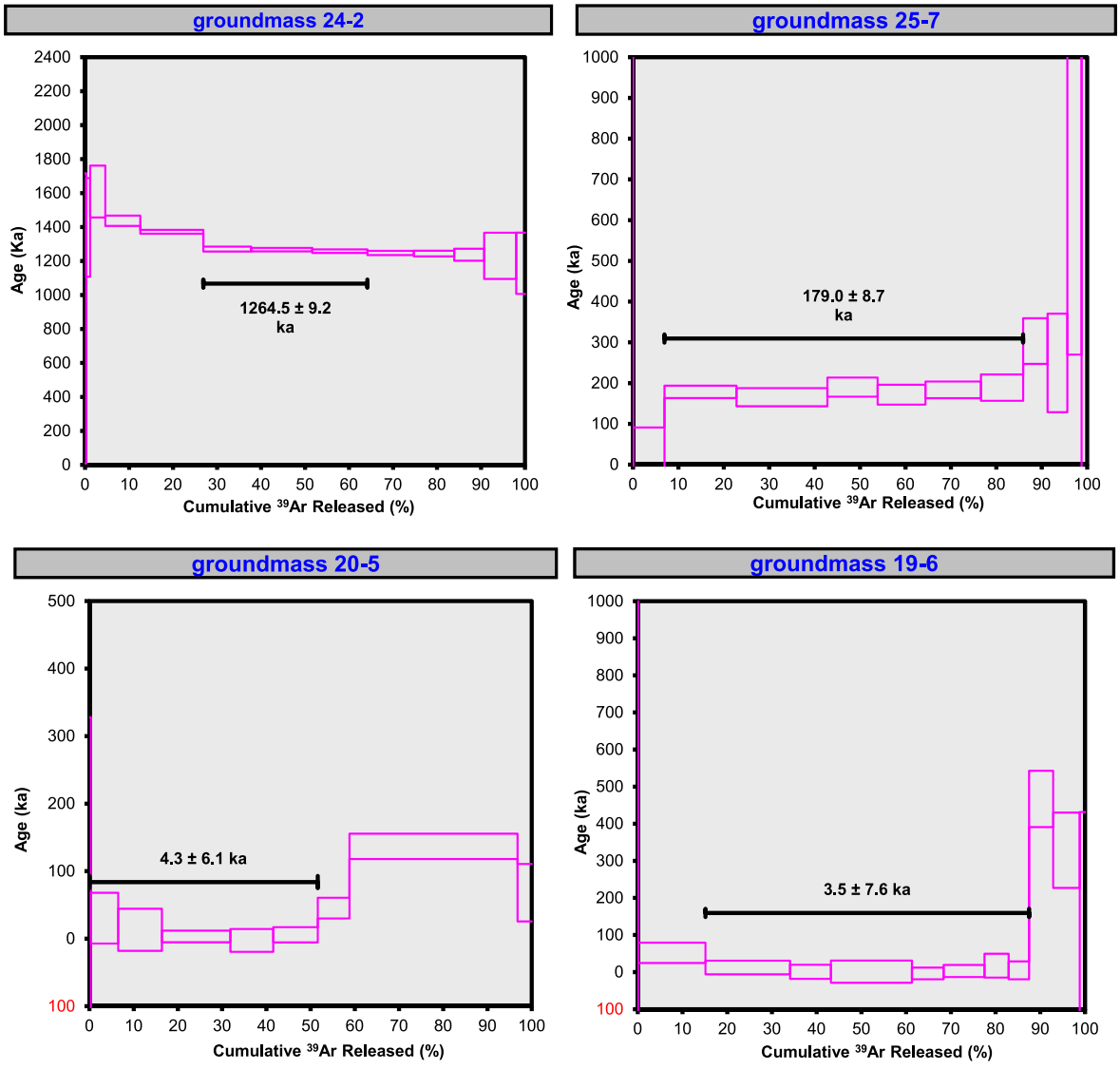

Fig. 6. Groundmass Ar/Ar incremental heating analysis showing age spectra. Sample KL2023-07-24-2 is first stage. Sample KL2023-07-25-7 is second stage. Samples KL2023-07-20-5 and KL2023-07-19-6- are third stage. All samples were analysed using Alder Creek sanidine (ACs) as a standard (Niespolo et al., 2017).

the larger errors mean that while the samples likely date from Holocene volcanism, the exact timing is less precise. Thus, while we interpret these ages as generally within the past 10,000 years, the exact eruption date is less constrained. The first and second stages have smaller relative errors, indicating more precise ages. Readers are directed to the literature for a more detailed explanation of how analytical errors are estimated in radiometric dating (Kelley, 2002).

2.9. Data obtained from EPMA and LA-ICP-MS

The distribution of the data points collected via EPMA and LA-ICP-MS based on the rock age is presented in Fig. 7. The LA-ICP-MS data demonstrates a balanced distribution while the EPMA data are less balanced as there is a small representation of the T3 age class (see Fig. 8).

3. Algorithm and implementation

3. Algorithm and implementation

The core objective of this research has been to evaluate the quality of the data obtained from the two analytical techniques discussed and assess the feasibility of training deep neural networks for AI-based age estimation of rocks once the analysis has been carried out. As such two separate modelling experiments were carried out. In one approach the objective was to assess whether a combination of a neural network model coupled with PCA dimensionality reduction and a machine learning unsupervised clustering technique able to classify the samples into three groups without any information associated with the rock age. The second approach involved training a neural network model with a portion of the data from each technique based on the age of the rocks and then assessing the model's performance in predicting the age of the rock associated with an unseen data set (see Fig. 9).

3.1. Experiment 1

The primary goal of this study was to determine if clustering algorithms could group rock samples into meaningful categories based on geochemical data obtained via EPMA and LA-ICP-MS. Specifically, the study evaluated whether these clusters aligned with the true age classes of the samples previously undertaken at the Geochronology Laboratory, CNR, Pisa. The methodology involved constructing an autoencoder to create a latent representation of the geochemical data and applying several clustering algorithms to the latent space. An autoencoder was built using TensorFlow to compress the geochemical data into a latent representation. The encoder reduced the dimensionality of the input data using dense layers with ReLU activation, creating a latent space represented by a 10-dimensional vector designed to capture the most significant patterns in the data. The decoder reconstructed the input data from the latent representation. The encoder was subsequently used to extract the latent space representation of the geochemical data. The structure of the model and data flow is illustrated in Fig. 10.

3.2. Experiment 2

In this study, we constructed a robust deep neural network (DNN) to classify the age of volcanic rocks using geochemical data derived from Laser Ablation Inductively Coupled Plasma Mass Spectrometry (LA-ICP-MS) and Electron Microprobe Analysis (EPMA). The data, encompassing (41 for LA-ICP-MS and 15 for EPMA) distinct geochemical features serves as a rich representation of the underlying mineralogical and elemental composition of the rocks, offering a reliable basis for age classification through supervised machine learning (Fig. 11).

The deep learning model was implemented using the TensorFlow Keras framework. A carefully designed sequential architecture was employed to ensure optimal learning and classification accuracy. The

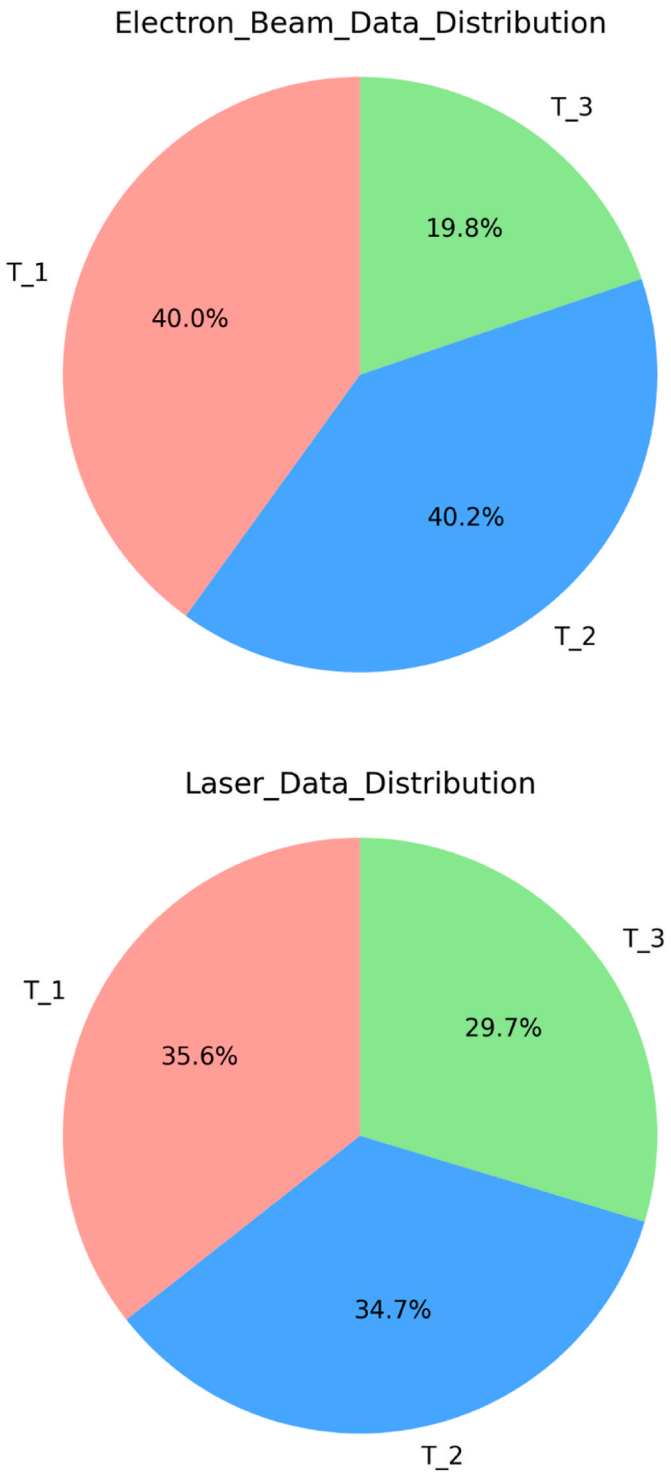

Fig. 7. Distribution of the data collected via the two techniques according to the rock age. T1 = first stage. T2 = second stage. T3 = third stage.

architecture is composed of the following layers:

3.2.1. Input layer

The input layer processes the relevant input geochemical features representing the rocks' elemental and mineralogical composition.

A dense layer with 64 neurons was employed, activated using the ReLU function to introduce non-linearity.

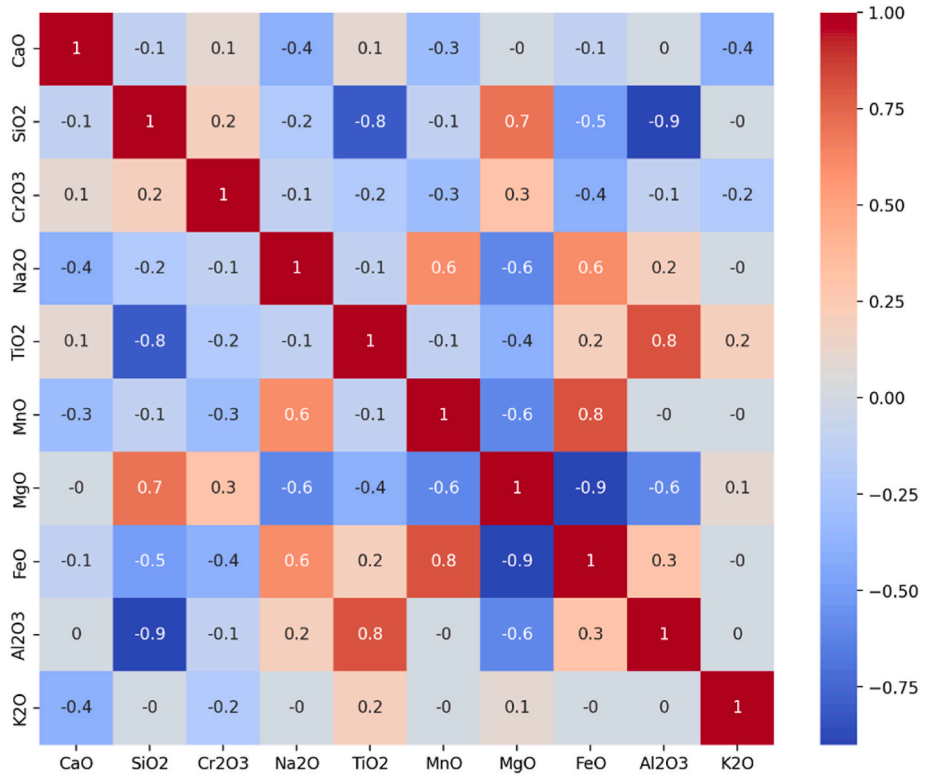

Fig. 8. Correlation matrix of the data associated with compounds quantified via EPMA.

3.2.2. Hidden layers

Three hidden layers were incorporated to extract complex patterns and interactions within the data: First Hidden Layer: 128 neurons with ReLU activation., Second Hidden Layer: 64 neurons with ReLU activation and a Third Hidden Layer: 32 neurons with ReLU activation.

Batch normalization layers were added after each dense layer to stabilize and accelerate training by normalizing the activations, thereby mitigating internal covariate shifts.

Dropout layers (30 % dropout rate) were interspersed to prevent overfitting by randomly deactivating a fraction of the neurons during training.

Output Layer: The final output layer consists of 3 neurons, each representing one of the predefined age categories. A softmax activation function was used to ensure the outputs are interpretable as probabilities, enabling classification into distinct age groups.

Optimization and Training; The network was optimized using the Adam optimizer with a multi stage finely tuned learning rate to balance convergence speed and precision. The categorical cross-entropy loss function was employed, reflecting the multi-class nature of the classification task. The model was trained to maximize classification accuracy, with training performance monitored through accuracy metrics on the training and validation datasets.

This DNN architecture demonstrates a sophisticated approach to leveraging geochemical datasets for geological investigations. By integrating techniques such as batch normalization and dropout, the model effectively balances learning capacity with generalization, making it a powerful tool for classifying the age of volcanic rocks.

4. Results

Several clustering algorithms were applied to the latent space, and their performance was compared using metrics such as Adjusted Rand Index (ARI), Homogeneity Score, and Adjusted Clustering Accuracy. Among these, k-means clustering was the best-performing technique. Further information on the above-mentioned metrics and their mathematical illustration is provided in the supplementary section of this report.

K-means assumes spherical clusters and evenly distributed cluster sizes, which seemed to align well with the nature of the dataset. Other methods, including Gaussian Mixture Models (GMM), DBSCAN, HDBSCAN, and Spectral Clustering, were also tested but did not outperform k-means due to the nature of the dataset and the assumptions underlying these algorithms. GMM, for instance, accounted for overlapping clusters but performed poorly compared to k-means, with weaker clustering performance reflected in lower accuracy and homogeneity scores.

To visualize the clustering results, the latent space was reduced to two dimensions using principal component analysis (PCA). True labels representing the age classes of the rock samples and predicted cluster labels were plotted for comparison. The visualizations provided a clear representation of how well the clusters aligned with the true labels. The clustering results are presented in Figs. 12 and 13 for the LA-ICP-MS and EPMA associated data.

Key findings demonstrated that considering the LA-ICP-MS, k-means clustering in the latent space of an autoencoder effectively grouped rock samples based on geochemical data, closely aligning with the true age classes. This outcome highlights the utility of combining deep learning techniques with traditional clustering methods in geochemical analyses. However, there is potential for further refinement. Future work could focus on optimizing the autoencoder architecture by experimenting with deeper or more complex models to improve latent space representation and testing different latent space dimensionalities. However, comparing clustering performance for EPMA and LA-ICP-MS data is interesting as it seems the EPMA data are incapable of providing enough information to the neural network to lead to a meaningful classification. This is highly important as it addresses the primary objective of this research.

The datasets used in this study for predicting the age of volcanic rocks were derived from two distinct analytical techniques- LA-ICP-MS and EPMA. While the EPMA dataset consisted of 417 samples, the LA-ICP-MS dataset included only 118 samples. It is acknowledged that

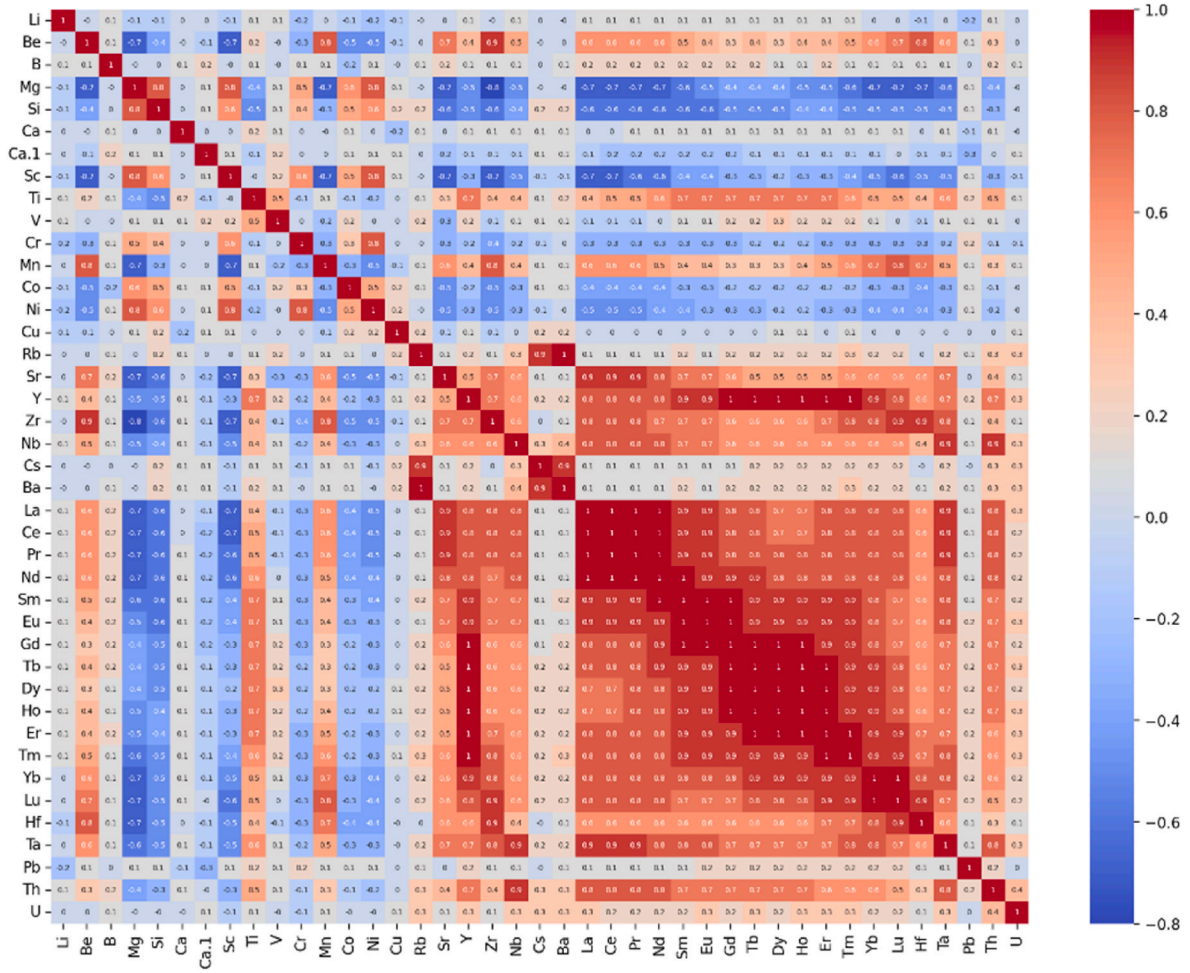

Fig. 9. Correlation matrix of the data associated with elements quantified via LA-ICP-MS.

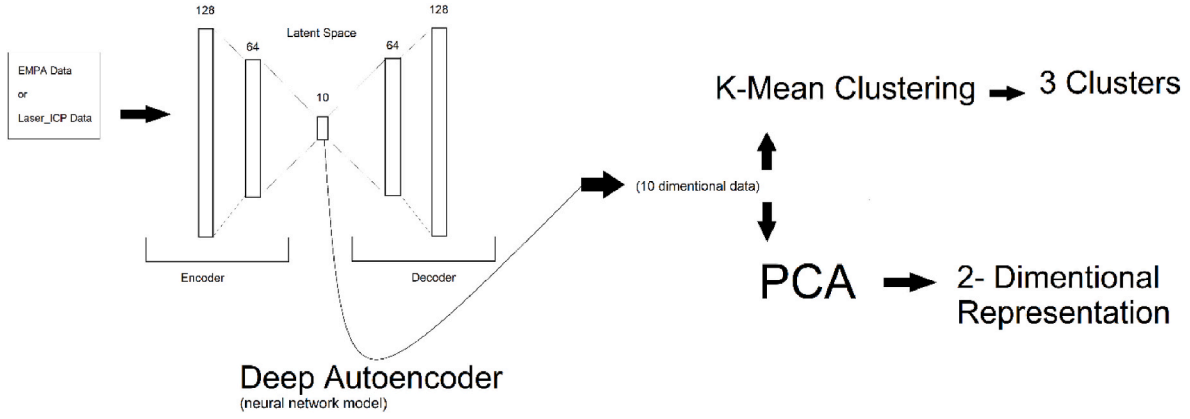

Fig. 10. The data is initially used to train an Autoencoder deep neural network. This configuration forms a latent lower (10D) dimensional representation of the original data. This lower dimensional data is then used for clustering via K means clustering algorithm and converted via principal component analysis into two-dimensional (2D) space for visualisation of the data.

the limited size of the latter dataset poses a potential challenge for training deep learning models, given the data-intensive nature of such approaches. However, it is important to note that obtaining high-quality geochemical data from these techniques is labour-intensive, time-consuming, and resource-intensive, often making large-scale data collection impractical. To ensure a fair and unbiased evaluation of the models, 10 % of the data was withheld as an unseen validation set in both cases. The results are presented in Fig. 14.

To further evaluate the performance of the classification models highlighted in Fig. 14, we computed additional metrics beyond overall accuracy, namely precision and recall for each class. Considering EMPA samples; the confusion matrix revealed that while the model achieved a satisfactory overall accuracy of 73.8 %, performance varied across age groups. Specifically, Class 1 yielded a precision of 0.714 and recall of 0.769, while Class 2 performed the best with a precision of 0.789 and recall of 0.833. In contrast, Class 3 showed a notably lower precision of

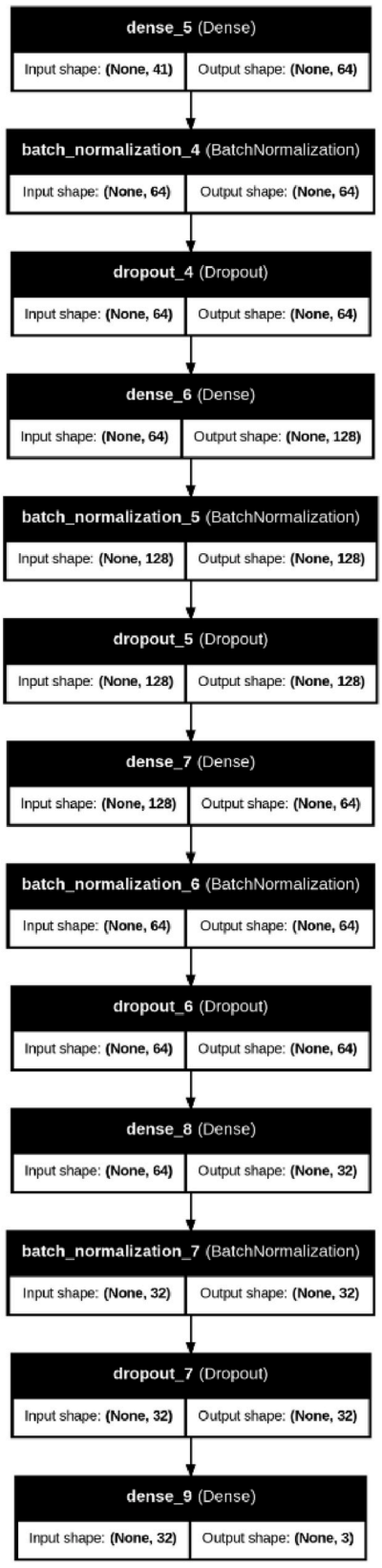

Fig. 11. Architecture of the deep neural network designed for classifying the age of volcanic rocks based on geochemical features obtained from EPMA and LA-ICP-MS. The model includes an input layer with 41 features, multiple hidden layers with batch normalization and dropout for improved generalization, and a SoftMax output layer for multi-class classification.

0.667 and recall of 0.545. This discrepancy suggests that the model had greater difficulty correctly identifying Holocene samples, likely due to overlaps in geochemical features or sample imbalance. These metrics highlight important areas for further refinement and support the need for future investigations into class-specific misclassifications and potential feature enhancements.

Despite the inherent data constraints, the LA-ICP-MS model achieved a remarkable classification accuracy of 95 %, significantly outperforming the EPMA-based model, which yielded an accuracy of 74 %. At first sight, this result highlights the potential of LA-ICP-MS data to provide superior discriminatory power for age classification, likely due to its ability to capture more detailed elemental signatures that are closely tied to the volcanic rocks' age.

In respect to LA_ICO_MS data, confusion matrix reveals high model performance with an overall accuracy of 95.8 %, indicating that the model can reliably classify rock samples into their correct age categories. Precision and recall offer deeper insight into per-class performance. Class shows a precision of 0.933 and perfect recall of 1.0, meaning that while a small number of misclassifications occurred from other classes being mistaken for Class 1, all actual Class 1 samples were correctly identified. Class 2 demonstrates perfect precision and recall (1.0), highlighting the model's flawless performance in both identifying and retrieving samples from this category. Class 3 also exhibits perfect precision (1.0), but a slightly lower recall (0.833) due to one misclassified instance. This suggests the model is conservative in assigning samples to Class 3, preferring not to risk false positives. These metrics demonstrate the model's robust and selective learning ability, with minimal overfitting, and highlight areas—particularly Class 3—where future refinement may enhance generalization.

The performance discrepancy is further illustrated in the respective confusion matrices, which provide a detailed breakdown of classification outcomes for each technique. The LA-ICP-MS confusion matrix demonstrates a high degree of precision and recall across all classes, underscoring its robustness even with a smaller dataset. Conversely, while the EPMA technique provides a broader dataset, its lower accuracy suggests that its geochemical measurements might lack the specificity required for precise age classification.

5. Conclusion

This study employed deep learning to classify volcanic rocks using geochemical data derived from two distinct analytical techniques and link these data to the rock's geochronology. The results revealed a striking disparity in classification performance, with LA-ICP-MS achieving an accuracy of 95 %, significantly outperforming the EPMA dataset, which yielded an accuracy of 72 %. While the differences in outcomes may initially appear surprising, they align well with the inherent characteristics of these techniques, the specific requirements of the classification task, and certain experimental conditions that warrant discussion.

The disparity in performance can be attributed to the fundamental differences between EPMA and LA-ICP-MS in terms of analytical capabilities. EPMA is primarily designed for the analysis of major and minor elements, focusing on spatial resolution at the micrometre scale. Although it provides valuable insights into the mineralogical composition of rocks, its limited ability to detect trace elements diminishes its suitability for age classification tasks. By contrast, LA-ICP-MS is specifically engineered to analyse a broad spectrum of trace elements at high sensitivity levels. Such trace elements often carry critical information related to magma source, evolution, and geodynamic processes thus the LA-ICP-MS dataset inherently provided a more informative and discriminative foundation for the classification model.

Another critical factor influencing these results is the difference in laboratory conditions under which the data were collected. The EPMA data was obtained from four different laboratories (Fig. 15), potentially introducing variability in the measurements due to differences in

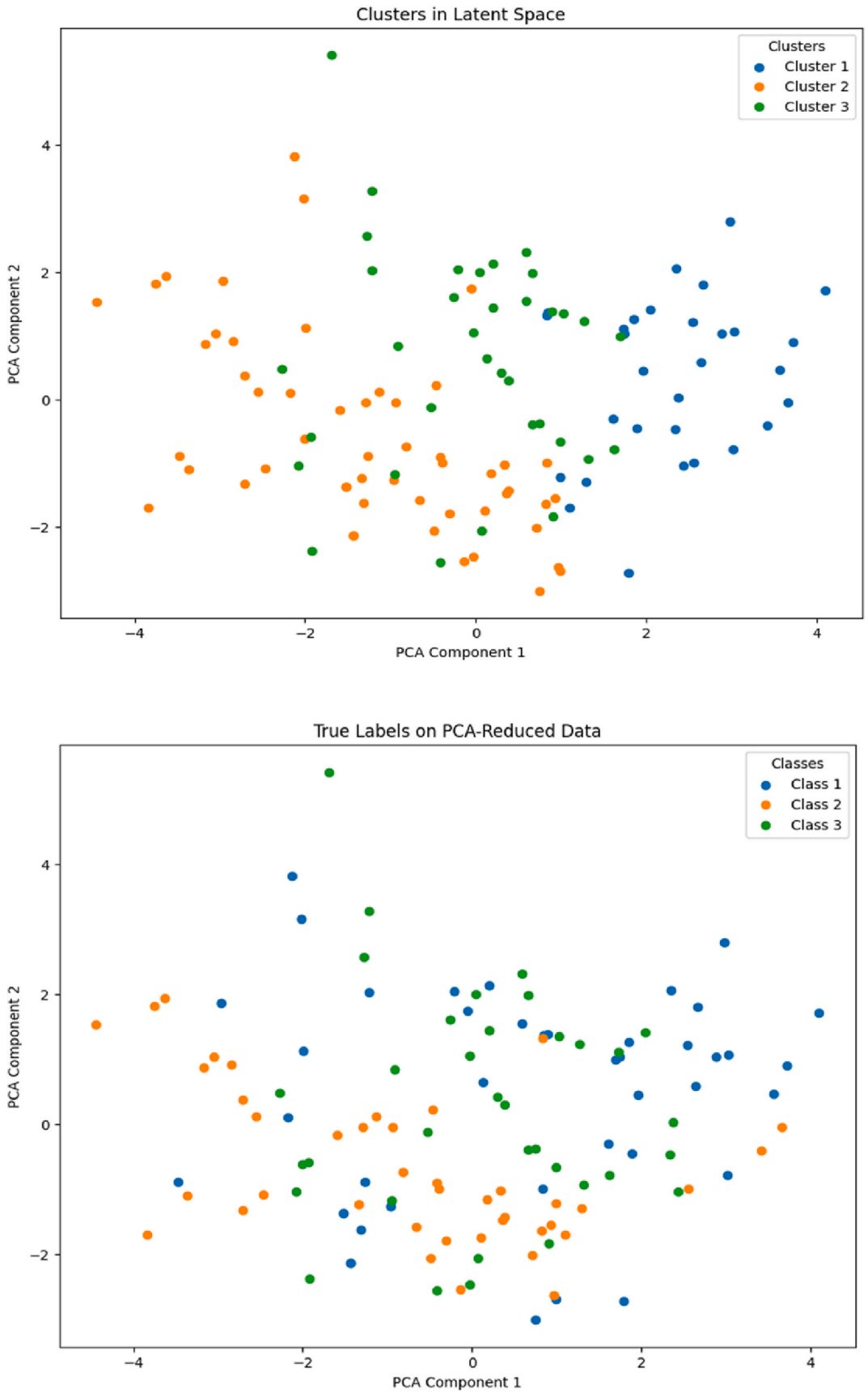

Fig. 12. Clustering of the LA-ICP-MS data after conversion into a 2-dimensional space. Top: Clusters based on the latent space. Bottom: Clusters based on the real age of the samples. The metrics associated with this experiment were: Adjusted Clustering Accuracy: 0.677, Adjusted Rand Index (ARI): 0.314, Homogeneity Score: 0.328.

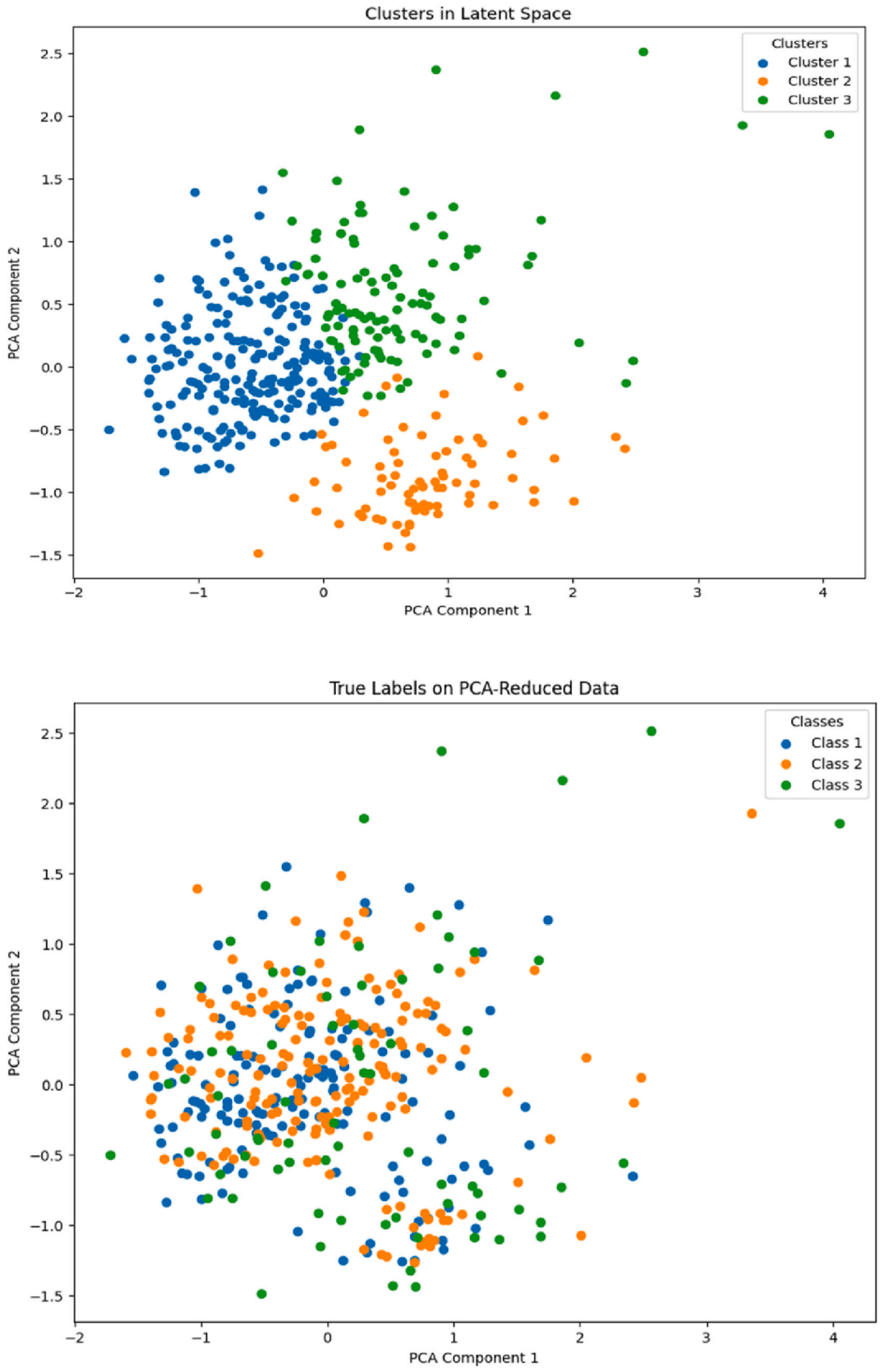

Fig. 13. Clustering of the EPMA data after conversion into a 2-dimensional space. Top: Clusters based on the latent space. Bottom: Clusters based on the real age of the samples. The metrics associated with this experiment were: Adjusted Clustering Accuracy: 0.458, Adjusted Rand Index (ARI): 0.036, Homogeneity Score: 0.028.

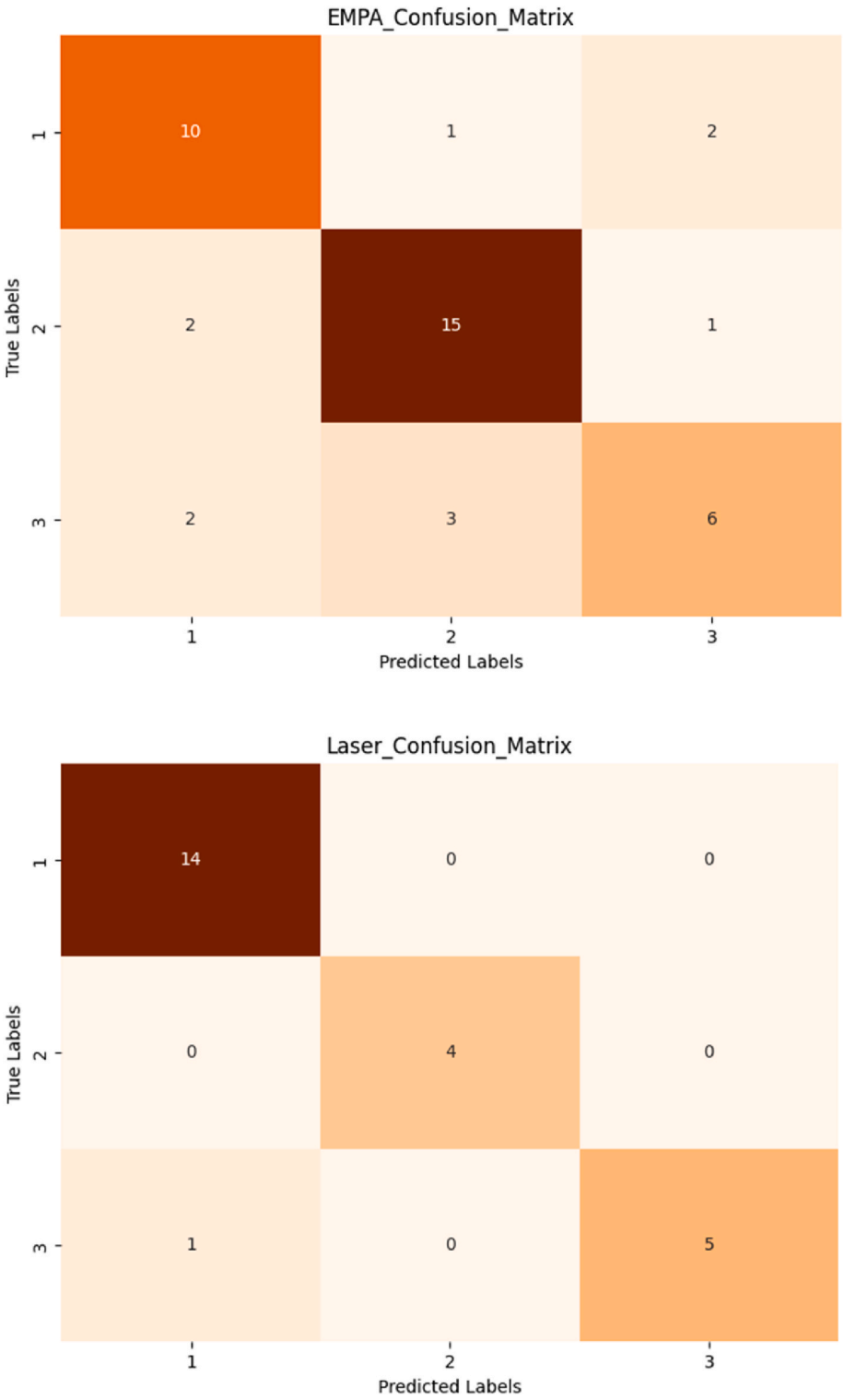

Fig. 14. Confusion matrices for the classification of volcanic rock ages using deep learning models. (Top): matrix represents results obtained using EPMA data, with a classification accuracy of 74 %. The bottom matrix corresponds to the LA-ICP-MS data, achieving a significantly higher accuracy of 95 %. The matrices illustrate the distribution of true versus predicted classifications, highlighting the superior performance of LA-ICP-MS in this study. The reported accuracies reflect the highest achieved across 10 separate train-test splits using randomly selected test sets. Across these runs, the lowest observed accuracy for the EMPA data was 68 %, while for the LA-ICP-MS data it was 91 %.

instrumentation, calibration protocols, and operator practices. Inter-laboratory variations are well-documented challenges in geochemical studies, as even minor differences in analytical setups can lead to inconsistencies in reported concentrations. Such variability can introduce noise into the EPMA dataset, reducing its overall utility for the ML model. The LA-ICP-MS data were obtained exclusively from a single laboratory, ensuring consistency in analytical conditions. This assumption can be overruled as we carried out the exact tests by training the same model with the EPMA exclusively obtained from each lab separately and an improvement was observed in the autoencoder model

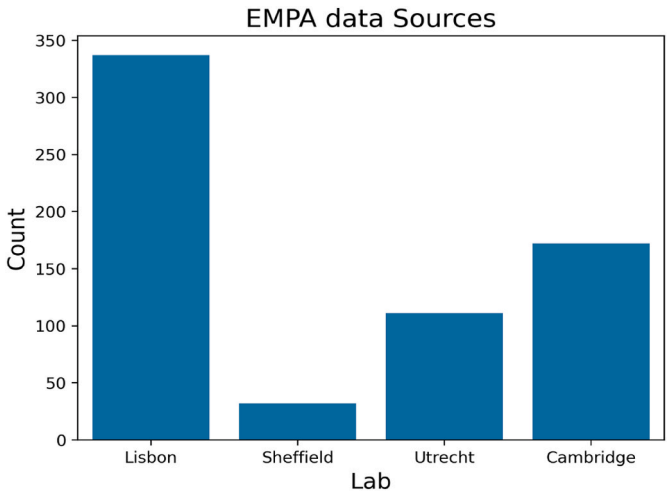

Fig. 15. The percentage of EPMA data from each of the four laboratories.

coupled with the PCA algorithm to construct a clustering mimicking the real class of the rock ages. These results are presented in the supplementary section.

However, it is also important to consider the practical challenges associated with data collection in geochemistry. While the EPMA dataset comprised 417 samples, the LA-ICP-MS dataset included only 118 samples. The limited size of the LA-ICP-MS dataset reflects the complexity and resource-intensive nature of obtaining such data in the laboratory. Despite these constraints, the LA-ICP-MS model outperformed the EPMA model, demonstrating the superior quality and relevance of its data for age classification tasks. Additionally, 10 % of the data was withheld as a test set in both cases, ensuring that the reported accuracies reflect the true predictive capabilities of the models.

The confusion matrices for the two techniques further illustrate the disparity in performance. The LA-ICP-MS confusion matrix demonstrates high precision and recall across all age classes, highlighting its robustness despite the smaller dataset size. In contrast, the EPMA confusion matrix reveals more frequent misclassifications, suggesting that the data lacked the granularity needed to differentiate between similar age categories effectively. These findings emphasize the importance of analytical technique selection in geochemical research and validate the transformative potential of advanced techniques such as LA-ICP-MS when paired with state-of-the-art ML models.

To successfully integrate AI and modern data analytics into the physical sciences, the quality and origin of the data cannot be overlooked. While many advocate for the creation of large data banks to advance this objective, our experiments highlight the challenges of using data sourced from multiple origins. Inconsistencies and variations in data quality can undermine the effectiveness of training ML models. Therefore, before compiling such datasets, it is crucial to establish standardized protocols and directives to ensure that data from diverse sources can be harmonized into a universal and reliable resource for model training. This foundational step will enable robust and reproducible AI-driven advancements in the physical sciences.

CRediT authorship contribution statement

Ali Salimian: Conceptualization, Software, Writing – original draft. **Megan Watfa:** Conceptualization, Data curation, Writing – review & editing. **Ram Grung:** Software, Validation. **Lorna Anguilano:** Investigation, Supervision, Writing – review & editing, Conceptualization.

Data and code availability section

The dataset used in this study, including Electron Microprobe and Laser Ablation Mass Spectroscopy results for volcanic rock dating, is available at Zenodo with DOI (10.5281/zenodo.1493329) under the CC-BY 4.0 license.

The Python scripts and Jupiter Notebooks used for data preprocessing, AI model training, and figure generation are available at GitHub and archived in Zenodo with DOI (10.5281/zenodo.14933482.

All datasets and software are shared under the MIT License, ensuring unrestricted access. Further methodological details, including data processing steps and AI model implementation, are provided in the Methods section.

Declaration of competing interest

The authors declare the following financial interests/personal relationships which may be considered as potential competing interests: Ali Salimian reports equipment, drugs, or supplies was provided by The Department of Earth Sciences, University of Cambridge. If there are other authors, they declare that they have no known competing financial interests or personal relationships that could have appeared to influence the work reported in this paper.

Acknowledgement

We acknowledge the support of the laboratories and institutions that contributed to this study: the Geolab Faculty of Geoscience Utrecht University, the Faculty of Sciences University of Lisbon, the Department of Earth Science University of Cambridge, the Sorby Centre for Electron Microscopy University of Sheffield, the Department of Earth Sciences University of Milan, and the Ar Ar Geochronology Laboratory, CNR, Pisa. Their assistance, guidance, and dedication have been deeply appreciated toward this research. We would also like to acknowledge the Quaternary Research Association, and the Mineralogical Society for their financial support.

Appendix A. Supplementary data

Supplementary data to this article can be found online at https://doi.org/10.1016/j.acags.2025.100263.

Data availability

Data will be made available on request.

References

Coble, M.A., Burgess, S.D., Klemetti, E.W., 2017. New zircon (U-Th)/He and U/Pb eruption age for the Rockland tephra, western USA. Quat. Sci. Rev. 172, 109–117. https://doi.org/10.1016/j.quascirev.2017.08.004.

Condomines, M., Gauthier, P.J., Sigmarsson, O., 2003. Timescales of magma chamber processes and dating of young volcanic rocks. Rev. Mineral. Geochem. 52 (1), 125–174. https://doi.org/10.2113/0520125.

Danišík, M., Schmitt, A.K., Stockli, D.F., Lovera, O.M., Dunkl, I., Evans, N.J., 2017. Application of combined U-Th-disequilibrium/U-Pb and (U-Th)/He zircon dating to tephrochronology. Quat. Geochronol. 40, 23–32. https://doi.org/10.1016/j.quageo.2016.07.005.

Das, R., Bhattacharyya, S., Nandy, S. (Eds.), 2020. Machine Learning Applications: Emerging Trends.

Di Vincenzo, G., 2007. 40 Ar-39 Ar dating by laserprobe. 40 Ar-39 Ar Dating by Laserprobe 1000–1006. https://doi.org/10.1400/114789.

Di Vincenzo, G., 2022. High precision multi-collector 40Ar/39Ar dating of moldavites (Central European tektites) reconciles geochrological and paleomagnetic data. Chem. Geol. 608, 121026. https://doi.org/10.1016/j.chemgeo.2022.121026.

Doglioni, C., Agostini, S., Crespi, M., Innocenti, F., Manetti, P., Riguzzi, F., Savascin, Y., 2002. On the extension in western Anatolia and the Aegean Sea. J. Virtual Explor. 8, 169–183. Previously 33.

Engi, M., Lanari, P., Kohn, M.J., 2017. Significant ages—An introduction to petrochronology. Rev. Mineral. Geochem. 83 (1), 1–12. https://doi.org/10.2138/rmg.2017.83.1.

Gennaro, E., Radica, F., Iezzi, G., Vetere, F., Nazzari, M., Zellmer, G.F., Scarlato, P., 2023. EPMA maps unveil the actual chemical variations and crystallisation sequence of pyroxene and plagioclase solidified from a basaltic liquid at variable cooling rates. Chem. Geol. 640, 121752. https://doi.org/10.1016/j.chemgeo.2023.121752.

Ginibre, C., Worner, G., Kronz, A., 2007. Crystal zoning as an archive for magma evolution. Elements 3 (4), 261–266. https://doi.org/10.2113/gselements.3.4.261.
Griffin, W.L., 2008. GLITTER: data reduction software for laser ablation ICP-MS. Laser Ablation ICP-MS in the Earth Sciences: Current Practices and Outstanding Issues, pp. 308–311.
Irvine, T.N., Baragar, W.R.A.F., 1971. A guide to the chemical classification of the common volcanic rocks. Can. J. Earth Sci. 8 (5), 523–548. https://doi.org/10.1139/e71-055.
Jaimes-Viera, M.D.C., Del Pozzo, A.M., Layer, P.W., Benowitz, J.A., Nieto-Torres, A., 2018. Timing the evolution of a monogenetic volcanic field: Sierra Chichinautzin, Central Mexico. J. Volcanol. Geoth. Res. 356, 225–242. https://doi.org/10.1016/j.jvolgeores.2018.03.013. Previously 32.
Jenner, F.E., O'Neill, H.S.C., 2012. Major and trace analysis of basaltic glasses by laser-ablation ICP-MS. G-cubed 13 (3). https://doi.org/10.1029/2011GC003890.
Jochum, K.P., Willbold, M., Raczek, I., Stoll, B., Herwig, K., 2005. Chemical characterisation of the USGS reference glasses GSA-1G, GSC-1G, GSD-1G, GSE-1G, BCR-2G, BHVO-2G and BIR-1G using EPMA, ID-TIMS, ID-ICP-MS and LA-ICP-MS. Geostand. Geoanal. Res. 29 (3), 285–302. https://doi.org/10.1111/j.1751-908X.2005.tb00901.x.
Kelley, S., 2002. K-Ar and Ar-Ar dating. Rev. Mineral. Geochem. 47 (1), 785–818. https://doi.org/10.2138/rmg.2002.47.17.
Kohn, M.J., Penniston-Dorland, S.C., 2017. Diffusion: obstacles and opportunities in petrochronology. Rev. Mineral. Geochem. 83 (1), 103–152. https://doi.org/10.2138/rmg.2017.83.4.
Le Bas, M.J., Le Maitre, R.N., Streckeisen, A., Zanettin, B., 1986. A chemical classification of volcanic rock based on total silica diagram. J. Petrol. 27 (3), 745–750. https://doi.org/10.1093/petrology/27.3.745.
Lee, T.H., Kwon, C.W., Ahn, U.S., Danišík, M., Lee, S., Yi, K., Guillong, M., 2024. A comparative study of different radiometric dating techniques applied to Quaternary volcanic rocks from Jeju island, South Korea. Geosci. J. 28 (5), 733–746. https://doi.org/10.1007/s12303-024-0024-2.
MacDonald, A., Ubide, T., Mollo, S., 2024. Degree of sector zoning in clinopyroxene records dynamic magma recharge and ascent. Geochem. Cosmochim. Acta 378, 245–258. https://doi.org/10.1016/j.gca.2024.06.025.
McDougall, I., Harrison, T.M., 1999. Geochronology and Thermochronology by the 40Ar/39Ar Method. Oxford University Press, USA.
Merrihue, C., Turner, G., 1966. Potassium-argon dating by activation with fast neutrons. J. Geophys. Res. 71 (11), 2852–2857. https://doi.org/10.1029/JZ071i011p02852.
Niespolo, E.M., Rutte, D., Deino, A.L., Renne, P.R., 2017. Intercalibration and age of the Alder Creek sanidine 40Ar/39Ar standard. Quat. Geochronol. 39, 205–213. https://doi.org/10.1016/j.quageo.2016.09.004.
Oggier, F., Widiwijayanti, C., Costa, F., 2023. Integrating global geochemical volcano rock composition with eruption history datasets. Front. Earth Sci. 11, 1108056. https://doi.org/10.3389/feart.2023.1108056. Previously 27.
Ouzounis, A.G., Papakostas, G.A., 2021. Machine learning in discriminating active volcanoes of the hellenic volcanic arc. Applied Sciences (Switzerland) 11 (18). https://doi.org/10.3390/app11188318.
Pearce, N.J., Perkins, W.T., Westgate, J.A., Gorton, M.P., Jackson, S.E., Neal, C.R., Chenery, S.P., 1997. A compilation of new and published major and trace element data for NIST SRM 610 and NIST SRM 612 glass reference materials. Geostand. Newsl. 21 (1), 115–144. https://doi.org/10.1111/j.1751-908X.1997.tb00538.x.
Petrelli, M., Bizzarri, R., Morgavi, D., Baldanza, A., Perugini, D., 2017. Combining machine learning techniques, microanalyses and large geochemical datasets for tephrochronological studies in complex volcanic areas: new age constraints for the Pleistocene magmatism of central Italy. Quat. Geochronol. 40, 33–44. https://doi.org/10.1016/j.quageo.2016.12.003.
Pignatelli, A., Piochi, M., 2021. Machine learning applied to rock geochemistry for predictive outcomes: the Neapolitan volcanic history case. J. Volcanol. Geoth. Res. 415, 107254. https://doi.org/10.1016/j.jvolgeores.2021.107254. Retrieved from.
Reiners, P.W., Campbell, I.H., Nicolescu, S., Allen, C.M., Hourigan, J.K., Garver, J.I., Cowan, D.S., 2005. (U-Th)/(He-Pb) double dating of detrital zircons. Am. J. Sci. 305 (4), 259–311. https://doi.org/10.2475/ajs.305.4.259.
Renne, P.R., Swisher, C.C., Deino, A.L., Karner, D.B., Owens, T.L., DePaolo, D.J., 1998. Intercalibration of standards, absolute ages and uncertainties in 40Ar/39Ar dating. Chem. Geol. 145 (1–2), 117–152. https://doi.org/10.1016/S0009-2541(97)00159-9.
Reyes-Guzmán, N., Siebe, C., Chevrel, M.O., Guilbaud, M.N., Salinas, S., Layer, P., 2018. Geology and radiometric dating of Quaternary monogenetic volcanism in the western Zacapu lacustrine basin (Michoacán, México): implications for archeology and future hazard evaluations. Bull. Volcanol. 80, 1–20. https://doi.org/10.1007/s00445-018-1193-5, 10.1007/s00445-018-11.
Schmidhuber, J., 2022. Annotated history of modern ai and deep learning. arXiv preprint arXiv:2212.11279. https://doi.org/10.48550/arXiv.2212.11279.
Schmitt, A.K., Martín, A., Stockli, D.F., Farley, K.A., Lovera, O.M., 2013. (U-Th)/He zircon and archaeological ages for a late prehistoric eruption in the Salton Trough (California, USA). Geology 41 (1), 7–10. https://doi.org/10.1130/G33634.1.
Shaaban, S.M., Tawfik, S.Z., 2020. Classification of volcanic rocks based on rough set theory. Eng. Technol. Appl. Sci. Res. 10 (2), 5501–5504. https://doi.org/10.48084/etasr.3420.
Sim, H., Jung, W., Hong, S., Seo, J., Park, C., Song, Y., 2022. Evaluating the effectiveness of an artificial intelligence model for classification of basic volcanic rocks based on polarized microscope image. Economic and Environmental Geology 55 (3), 309–316. https://doi.org/10.9719/EEG.2022.55.3.309.
Smellie, J.L., Martin, A.P., Di Vincenzo, G., Townsend, D.B., Heizler, M.T., Ruth, D.C., 2022. Eruptive history of Mason Spur, a Miocene—Pleistocene polygenetic volcanic complex in southern Victoria Land, West Antarctic Rift System, Antarctica. Bull. Volcanol. 84 (10), 93. https://doi.org/10.1007/s00445-022-01601-4.
Tokçaer, M., Agostini, S., Savaşçin, M.Y., 2005. Geotectonic setting and origin of the youngest Kula volcanics (western Anatolia), with a new emplacement model. Turk. J. Earth Sci. 14 (2), 143–166. Previously 31.
Uslular, G., Kıyıkçı, F., Karaarslan, E., Kuşcu, G.G., 2022. Application of machine-learning algorithms for tephrochronology: a case study of Plio-Quaternary volcanic fields in the South Aegean Active Volcanic Arc. Earth Science Informatics 15 (2), 1167–1182. https://doi.org/10.1007/s12145-022-00797-5.
Walters, J.B., Cruz-Uribe, A.M., Song, W.J., Gerbi, C., Biela, K., 2022. Strengths and limitations of in situ U–Pb titanite petrochronology in polymetamorphic rocks: an example from western Maine, USA. J. Metamorph. Geol. 40 (6), 1043–1066. https://doi.org/10.1111/jmg.12657.
Wu, S., Wörner, G., Jochum, K.P., Stoll, B., Simon, K., Kronz, A., 2019. The preparation and preliminary characterisation of three synthetic andesite reference glass materials (ARM-1, ARM-2, ARM-3) for in situ microanalysis. Geostand. Geoanal. Res. 43 (4), 567–584. https://doi.org/10.1111/ggr.12301.
Yang, F., Zuo, R., Kreuzer, O.P., 2024. Artificial intelligence for mineral exploration: a review and perspectives on future directions from data science. Earth Sci. Rev., 104941 https://doi.org/10.1016/j.earscirev.2024.104941.
Zawacki, E.E., van Soest, M.C., Hodges, K.V., Scott, J.J., Barboni, M., Strecker, M.R., Arrowsmith, J.R., 2022. Sediment provenance and silicic volcano-tectonic evolution of the northern east African rift system from U/Pb and (U-Th)/He laser ablation double dating of detrital zircons. Earth Planet Sci. Lett. 580, 117375. https://doi.org/10.1016/j.epsl.2022.117375.
Zhang, P., Zhang, Z., Yang, J., Cheng, Q., 2023. Machine learning prediction of ore deposit genetic type using magnetite geochemistry. Natural Resources Research 32 (1), 99–116. https://doi.org/10.1007/s11053-022-10146-4. Retrieved from.